Effects of Wave Breaking on the Near-Surface Profiles of Velocity and Turbulent Kinetic Energy

ARNE MELSOM AND ØYVIND SÆTRA*

Norwegian Meteorological Insitute, Oslo, Norway

(Manuscript received 27 March 2002, in final form 24 July 2003)

ABSTRACT

A theoretical model for the near-surface velocity profile in the presence of breaking waves is presented. Momentum is accumulated by growing waves and is released upon wave breaking. In effect, such a transition is a process involving a time-dependent surface stress acting on the mean current. In this paper, conventional theory for the Stokes drift is expanded to fourth-order accuracy in wave steepness. It is shown that the higher-order terms lead to an enhancement of the surface Stokes drift and a slight retardation of the Stokes volume flux. Furthermore, the results from the wave theory are used to obtain a bulk parameterization of momentum exchange during the process of wave breaking. The mean currents are then obtained by application of a variation of the ''level 2.5'' turbulence closure theory of Mellor and Yamada. When compared with the traditional approach of a constant surface stress, the mean Eulerian current exhibits a weak enhancement in the near-surface region, compensated by a negative shift deeper in the water column. However, it is found that the results of Craig and Banner and the results of Craig are not significantly affected by the present theory. Hence, this study helps to explain why the Craig and Banner model agrees well with observations when a realistic, time-varying surface stress acts on the drift currents.

1. Introduction

With the exception of coastal regions with large tidal amplitudes, the circulation of the ocean's surface layer is mainly attributed to the wind stress. This stress induces motion in the upper ocean on a variety of scales, ranging from turbulence to waves and ocean currents. The effect of the wind stress on waves can be observed as increasing wave amplitudes. This process has limitations, since waves with a steepness beyond a critical value become unstable and wave breaking occurs. The main topics of the present paper are 1) how wave breaking affects the distribution of the momentum input to the ocean due to a stress acting on the free ocean surface and 2) how wave breaking affects the near-surface properties of turbulence.

For a given stress at the ocean's surface, the vertically integrated momentum in the ocean is influenced only by the momentum sink at the bottom. Obviously, this is also true when momentum is distributed between wave motion and mean currents (Weber and Melsom 1993a). However, the presence of waves and wave breaking may significantly affect the vertical distribution of momentum and its temporal evolution (Melsom 1996).

In a study that has a focus on the distribution of momentum, the description of mixing processes plays an essential role. Recently, a generalization of well-known turbulence closure models (TCMs) has been developed by Umlauf and Burchard (2003). The widely used turbulence closure model by Mellor and Yamada (1982) (MY-TCM) is one of the models that can be retrieved as a special case of Umlauf and Burchard's generic model.

In their study, Craig and Banner (1994, hereinafter CB) examine wave-enhanced turbulence by application of the Mellor–Yamada model. The effect of waves is parameterized by adoption of an alternative expression for the relation between the wind stress and the turbulent kinetic energy (TKE) at the surface. Moreover, CB consider simplifications of the MY-TCM and find that the traditional law-of-the-wall assumption of shear production of TKE being balanced by dissipation does not apply in a wave-enhanced surface layer.

Numerical modeling of ocean circulation is one field in which the presence of waves and wave breaking is largely ignored. For model results regarding features like the large-scale and the mesoscale ocean circulation, the omission of effects of wave breaking is not expected to be a matter of concern in the present context. However, when information in the near-surface region (on a

* Current affiliation: European Centre for Medium-Range Weather Forecasts, Reading, United Kingdom.

Corresponding author address: Arne Melsom, Norwegian Meteorological Institute, P.O. Box 43, Blindern, N-0313 Oslo, Norway.
E-mail: arne.melsom@met.no

vertical scale corresponding to the length of gravity waves or shorter) is pertinent, the presence of breaking waves may potentially have an impact on the model results. This may be the case for models that use terrain-following coordinates in the vertical, such as the Princeton Ocean Model (Mellor 1992) and the *S*-Coordinates Rutgers University Model (Song and Haidvogel 1994). When such models are applied to domains that span depths from a few tens of meters to thousands of meters, the uppermost layers in shallow waters may well have a thickness in the range 0.1–1 m. Traditional numerical ocean circulation models that are formulated with a z coordinate in the vertical, for example, Cox and Bryan (1984), may also have a resolution of a few meters (or less) in the uppermost model layer. This is also the case for a class of emerging circulation models that are formulated with a hybrid coordinate in the vertical (e.g., Bleck 2002). For a model that includes near-surface dynamics, it may be important to incorporate a realistic parameterization of wave breaking. For models with lower vertical resolution, rather than changing the model parameterization, effects of wave breaking may need to be considered if the surface velocity is derived from the results for the upper model layer. In the context of local redistribution of momentum, effects of wave breaking can safely be ignored when predictions in the deeper parts of the ocean are considered.

It is a formidable task to provide a detailed description of wave breaking and how it affects currents and turbulence. In the present paper, no efforts will be made toward such an end. Instead, effects of wave breaking will be parameterized as described in Melsom (1996), utilizing the conservation properties of mass and momentum. In that paper, it was found that wave breaking enhances the surface drift. However, vertical diffusion of momentum by turbulence was parameterized using an eddy viscosity of constant value. In the present paper, the aim is at a realistic description of vertical momentum diffusion by invoking a version of the MY-TCM (Mellor 1973; Mellor and Yamada 1974, 1982) with the modifications related to wave enhancement that were suggested by CB.

Craig and Banner (1994) find that the Mellor–Yamada model, with their modifications, shows ''agreement in detail with measured profiles of dissipation,'' despite the fact that the model is not parameterized or calibrated to describe drift currents in a sea state that is influenced by breaking waves. This is particularly the case for the relatively short period from when an isolated wave breaking event occurs to the time when the wave's mass and momentum have been redistributed. One important goal in this study is to investigate how isolated wave breaking events affect the balance of the terms in the equation for the TKE, by application of a bulk parameterization of the effects of mass and momentum redistribution.

The second important goal is to obtain results that may hold valuable information to the numerical ocean circulation modeling community with respect to the need, or lack of need, for parameterization of the subscale process of wave breaking. The effect of wave breaking on the ocean's surface drift will be assessed in this context.

2. Mathematical formulation

The present theory includes diverse features of the ocean circulation, namely, a TCM, an investigation of wave motion to fourth order in wave steepness, and a description of mean currents. Wave motion, mean motion, and high-frequency motion are separated as described, for example, by Weber and Melsom (1993a). Assuming that distinct time scales exist, the Eulerian pressure and velocity fields are divided into three separate parts:

$$(p, \mathbf{v}) = (p', \mathbf{v}') + (\hat{p}, \hat{\mathbf{v}}) + (\overline{p}, \overline{\mathbf{v}}). \tag{1}$$

Here primes, carets, and overbars denote small-scale turbulent fluctuations, wave motion, and mean motion, respectively. The governing equations for the wave motion and for the mean motion are developed by application of time averaging. Two time-averaging processes are employed. They are denoted by angle brackets and braces and correspond to integration over periods that remove linear turbulent and linear wave quantities, respectively.

The present study is confined to the upper layer of the ocean where the density ρ is taken to be constant. Furthermore, effects of molecular viscosity are omitted because of the small magnitude of the viscosity. A Cartesian frame of reference is applied with the vertical z axis being positive upward. The undisturbed horizontal surface is taken to define $z = 0$. The governing Eulerian equations for wave motion and mean motion then become

$$\frac{\partial \hat{\mathbf{v}}}{\partial t} + \hat{\mathbf{v}} \cdot \boldsymbol{\nabla}\hat{\mathbf{v}} - \{\hat{\mathbf{v}} \cdot \boldsymbol{\nabla}\hat{\mathbf{v}}\} = -\boldsymbol{\nabla}\frac{\hat{p}}{\rho} + \boldsymbol{\nabla} \cdot (-\hat{\mathbf{v}}\overline{\mathbf{v}} - \overline{\mathbf{v}}\hat{\mathbf{v}} - \langle \mathbf{v}'\mathbf{v}' \rangle + \{\langle \mathbf{v}'\mathbf{v}' \rangle\}) \tag{2}$$

and

$$\frac{\partial \overline{\mathbf{v}}}{\partial t} + \overline{\mathbf{v}} \cdot \boldsymbol{\nabla}\overline{\mathbf{v}} = -\boldsymbol{\nabla}\frac{\overline{p}}{\rho} - g\mathbf{k} + \boldsymbol{\nabla} \cdot (-\{\langle \mathbf{v}'\mathbf{v}' \rangle\} - \{\langle \hat{\mathbf{v}}\hat{\mathbf{v}} \rangle\}), \tag{3}$$

respectively. Here g is the vertical acceleration due to gravity, and $\boldsymbol{\nabla}$ denotes the gradient operator. Details on the derivation of these equations are given by Weber and Melsom (1993a).

Note that effects of the earth's rotation have been disregarded. If such effects were to be taken into account, the wave field also becomes affected when the wave propagation direction is constant in a rotating

frame of reference (Hasselmann 1970). Then, vorticity is introduced into the wave equations, introducing an additional complexity to the already fairly intricate wave theory that is presented in appendix A. This simplification implies restriction with respect to the validity of the results beyond the first few hours of integration.

3. Turbulence and Reynolds stresses

The presence of turbulence gives rise to Reynolds stresses in (3). We shall adopt the description of these stresses as outlined by Craig (1996, hereinafter C96). This description involves use of an eddy viscosity ν:

$$-\{\langle u'w'\rangle\} = \nu\frac{\partial\overline{u}}{\partial z}. \tag{4}$$

Moreover, the eddy viscosity is defined by

$$\nu = lqS_M, \tag{5}$$

where l is a reference length scale for turbulent fluctuations.

Introducing the MY-TCM, S_M is a parameter with a constant value in the present case of unstratified water. Moreover, we apply their ''level 3'' equation for the turbulent kinetic energy (TKE), $q^2/2$. If we neglect advection of TKE and introduce (4) and (5), we have

$$\frac{\partial}{\partial t}\left(\frac{q^2}{2}\right) = \frac{\partial}{\partial z}\left[lqS_q\frac{\partial}{\partial z}\left(\frac{q^2}{2}\right)\right] + lqS_M\left(\frac{\partial\overline{u}}{\partial z}\right)^2 - \frac{q^3}{Bl}. \tag{6}$$

Here S_q and B are additional empirical constants. Note also that, in the absence of stratification, the level-3 version for turbulence closure is identical to the popular ''level 2.5'' version (Mellor and Yamada 1982). Hereinafter, q will be referred to as the scaling velocity for turbulence.

The reference turbulence length scale l is taken to increase linearly from the surface toward the interior of the ocean (e.g., Prandtl 1952):

$$l = \kappa(z_r - z): \tag{7}$$

where κ is von Kármán's constant and z_r is the surface roughness length.

In the presence of breaking waves, observations indicate that the TKE flux at the surface can be parameterized as

$$lqS_q\frac{\partial}{\partial z}\left(\frac{q^2}{2}\right) = \alpha u_*^3, \qquad z = 0 \tag{8}$$

(see CB), where u_* is the friction velocity due to the wind stress that acts on the ocean's surface, and α is a parameter that is generally a function of the sea state (Drennan et al. 1992).

4. Waves

a. Wave motion

As in Weber and Melsom (1993a), motion associated with a surface wave that travels in the x direction is considered:

$$\zeta = \zeta_0 e^{\beta t}[\cos(kx - \omega t) + O(k\zeta_0)], \tag{9}$$

where k is the wave number, ω is the frequency, β is an exponential growth rate, and ζ_0 is the initial surface amplitude of the gravest mode. The wave motion and the dispersion relation $\omega(k)$ are then found by solving (2) and the corresponding mass conservation equation with appropriate boundary conditions.

The wave motion is governed by (2) and the mass conservation equation. For the separation (1) to be meaningful, we must have $\nabla\cdot\langle\mathbf{v}'\mathbf{v}'\rangle \sim \mathbf{A}\cos\omega t + \mathbf{B}$. Furthermore, it is assumed that there is a relatively small contribution from the Reynolds stress terms $\langle\mathbf{v}'\mathbf{v}'\rangle$ at frequencies close to ω, that is, $|\mathbf{A}| \ll |\mathbf{B}|$. Then, the two terms in (2) that involve the Reynolds stresses will tend to cancel each other since

$$\nabla\cdot(-\langle\mathbf{v}'\mathbf{v}'\rangle + \{\langle\mathbf{v}'\mathbf{v}'\rangle\}) \sim -\mathbf{A}\cos\omega t.$$

Hence their combined effect on the wave motion will be neglected in (2). Moreover, the nonlinear terms involving $\hat{\mathbf{v}}$ and $\overline{\mathbf{v}}$ in (2) are neglected. This will restrict the accuracy of the description of the wave field close to breaking.

The above approximations are the same as in Melsom (1996). Equation (2) can now be written

$$\frac{\partial\hat{\mathbf{v}}}{\partial t} + \hat{\mathbf{v}}\cdot\nabla\hat{\mathbf{v}} - \{\hat{\mathbf{v}}\cdot\nabla\hat{\mathbf{v}}\} = -\nabla\frac{\hat{p}}{\rho}. \tag{10}$$

If the wave field has no vorticity initially, it remains irrotational. In this case the velocity field can be represented by a potential function φ as $\hat{\mathbf{v}} = \nabla\varphi$, and the solution for exponentially growing waves is given in appendix A. Since the results arise from inviscid theory, wave growth is produced by a surface pressure perturbation that is out of phase with the surface shape and in phase with the vertical velocity of the ocean waves. Then, the surface pressure acts in the direction of the fluid motion, adding energy to the ocean in terms of an increased wave height.

b. Higher-order wave drift

The particle drift may be derived in a Lagrangian manner, following the method outlined by Lamb (1932). This method is formulated as a computation of the mass transport below material interfaces that are horizontal in the absence of waves. The shape of material interfaces η may be derived, for example, by integration of the continuity equation:

$$\int_{-\infty}^{\eta} \frac{\partial^2 \varphi}{\partial x^2}\, dz = -\frac{\partial \varphi}{\partial z}(z = \eta) = -\frac{\partial \eta}{\partial t} - \frac{\partial \varphi}{\partial x}(z = \eta)\frac{\partial \eta}{\partial x}. \quad (11)$$

Observing that the surface is a material interface, we find that the shape of η to $O(\varepsilon^3)$ is

$$\eta = z_0 + k^{-1}\left\{\varepsilon \cos\theta e^{kz_0} + \varepsilon^2 \frac{1}{2}\cos(2\theta)e^{2kz_0} + \varepsilon^3\left[\frac{3}{8}\cos(3\theta) + \frac{5}{8}\cos\theta\right]e^{3kz_0} - \varepsilon^3\left(\frac{5}{8}\cos\theta - B\sin\theta\right)e^{kz_0}\right\}. \quad (12)$$

Here, $\varepsilon = k\zeta_0 e^{\beta t}$ is a nondimensional measure of the wave steepness, $\theta = kx - \omega t$ is the phase function, and z_0 is the vertical position of the interface when at rest. The Eulerian periodic velocity profile is given by (A7) in appendix A, and the mass transport below the interface η is

$$U(z < \eta) = \int_{-\infty}^{\eta} \frac{\partial \varphi}{\partial x}\, dz. \quad (13)$$

After some rather tedious arithmetic, we find that the mean Lagrangian transport below η becomes

$$\overline{U(z < z_0)} = \frac{1}{2}\varepsilon^2 c_0 k^{-1} e^{2kz_0} + \varepsilon^4 c_0 k^{-1}\left(\frac{1}{2}e^{4kz_0} - \frac{3}{8}e^{2kz_0}\right), \quad (14)$$

where the overbar denotes a mean quantity that results from an average over the period of the gravest wave mode, as defined in section 2. Also, $c_0 = \sqrt{g/k}$ is the lowest-order phase velocity, as defined in appendix A.

The Stokes drift $\overline{u}_S$, which is the mean drift velocity of particles in a nonrotating inviscid fluid, is then given to fourth order in wave amplitude as

$$\overline{u}_S(z_0) = \frac{d}{dz}\overline{U(z < z_0)} = \varepsilon^2 c_0 e^{2kz_0} + \varepsilon^4 c_0\left(2e^{4kz_0} - \frac{3}{4}e^{2kz_0}\right). \quad (15)$$

The Stokes drift has also been calculated by an Eulerian approach in which the particles' trajectories were derived using Taylor series expansions in time. This approach led to a number of terms that grow linearly in time and was not suited for determination of a mean property such as the Stokes drift. However, the terms that contained periodic and constant multipliers of powers of ε were in concord with (15).

5. Parameterization of wave breaking

The process of breaking of a monochromatic wave will be parameterized by requiring conservation of mass and momentum. This approach was described by Melsom (1996), using second-order accuracy in the underlying wave theory. Here, the same method is applied, and the analysis is extended to fourth-order accuracy in wave steepness. This constitutes an appropriate extension of the earlier work since wave breaking is closely associated with steep waves.

Effects of one isolated wave breaking event are examined. Let ΔM_E be the amount of Eulerian momentum that is lost from the wave motion when the amplitude is reduced by $\Delta\zeta$ to ζ_0. Then,

$$\Delta M_E = \int_{-\infty}^{\zeta_0+\Delta\zeta} \hat{u}(x, z, t; \varepsilon_0 + \Delta\varepsilon)\, dz - \int_{-\infty}^{\zeta_0} \hat{u}(x, z, t; \varepsilon_0)\, dz$$

$$\Rightarrow \overline{\Delta M_E} = \rho c_0 k^{-1}\Delta\varepsilon\left(\varepsilon_0 + \frac{1}{2}\Delta\varepsilon + \frac{1}{2}\varepsilon_0^3\right) = \overline{\Delta M_1} + \overline{\Delta M_2(z < \zeta)}, \quad (16)$$

where $\hat{u}(x, z, t; \varepsilon)$ is the velocity in the x direction that is associated with waves of a steepness ε, $\varepsilon_0 = \zeta_0 k$ is the wave steepness after breaking, $\Delta\varepsilon = \Delta\zeta k$ is the reduction in wave steepness due to breaking, and ΔM_1 and ΔM_2 are defined below.

As a consequence of reduction in amplitude, momentum associated with periodic motion is lost at the surface. Here, mass is redistributed by wave breaking in a process that can be observed as white capping. In a sense, mass moving in the wave's propagation direction (dark shading in Fig. 1a) is replaced by mass moving in the opposite direction (light shading in Fig. 1a). We denote the momentum transfer associated with this process by ΔM_1. Hence, this quantity represents the momentum deficit due to the redistribution of mass at the surface that is associated with white capping, and we find

$$\Delta M_1 = \rho \int_{\zeta_0}^{\zeta_0+\Delta\zeta} \hat{u}(x, z, t; \varepsilon_0 + \Delta\varepsilon)\, dz$$

$$\Rightarrow \overline{\Delta M_1} = \frac{1}{2}\rho c_0 k^{-1}\Delta\varepsilon(\varepsilon_0 + \Delta\varepsilon + \varepsilon_0^3), \qquad (17)$$

where ζ_0 is the shape of the surface for a monochromatic wave with steepness ε_0 and ζ is given by (A8) in appendix A.

Moreover, the changes in the pressure gradient due to wave breaking will give rise to an instantaneous adjustment of the wave motion in the entire water column. The amount of Eulerian momentum that is lost from the waves beneath the interface level after wave breaking becomes

$$\Delta M_2[z < \eta(x, z_0, t; \varepsilon_0)] = \rho \int_{-\infty}^{\eta(x,z_0,t;\varepsilon_0)} [\hat{u}(x, z, t; \varepsilon_0 + \Delta\varepsilon) - \hat{u}(x, z, t; \varepsilon_0)]\, dz$$

$$\Rightarrow \overline{\Delta M_2(z < \eta)} = \frac{1}{2}\rho c_0 k^{-1}\varepsilon_0\Delta\varepsilon[(1 - \varepsilon_0^2)e^{2kz_0} + \varepsilon_0^2 e^{4kz_0}], \qquad (18)$$

where the shape of the material interface η is given by (12). The vertical distribution of $\overline{\Delta M}_2$ is indicated by the shaded area in Fig. 1b.

In the present formulation, all of the momentum that is lost from the wave motion must be transferred to the mean motion. For the Stokes drift given by (15) we obtain

$$\Delta\overline{u}_S = -2c_0\Delta\varepsilon\left[\left(\varepsilon_0 + \frac{1}{2}\Delta\varepsilon - \frac{3}{2}\varepsilon_0^3\right)e^{2kz} + 4\varepsilon_0^3 e^{4kz}\right]$$

$$\Rightarrow \rho\int_{-\infty}^{0} \Delta\overline{u}_S\, dz' = -\overline{\Delta M_E}, \qquad (19)$$

and so the momentum transferred to the mean Eulerian motion is exactly compensated by a reduction in the Stokes drift. Thus, the vertically integrated Lagrangian momentum is not affected by wave breaking (Weber and Melsom 1993a).

Transfer of momentum lost from the periodic motion at the surface, ΔM_1, may be parameterized by a virtual wave stress τ_{vw} acting on the mean current at the surface. Such a parameterization was first suggested by Longuet-Higgins (1969) in a study of decaying waves. When wave breaking occurs at $t = 0$, we then obtain

$$\tau_{vw} = F(\omega t)\overline{\Delta M_1}, \qquad \int_0^\infty F(t')\, dt' = 1. \qquad (20)$$

In the case of breaking waves, the weight function $F(t)$ must go rapidly to 0, that is, with an exponential decay rate of one wave period or so. There is no obvious choice for the temporal development of the virtual wave stress due to breaking, τ_{vw}. However, in Melsom (1996) two extreme choices for F in (20) were investigated, namely, the delta function and an exponential decay rate set to the wave period. It was shown that the effects of wave breaking are relatively insensitive to the choice for F. For this reason, only the delta function will be implemented in the present study.

The momentum transfer associated with the adjustment

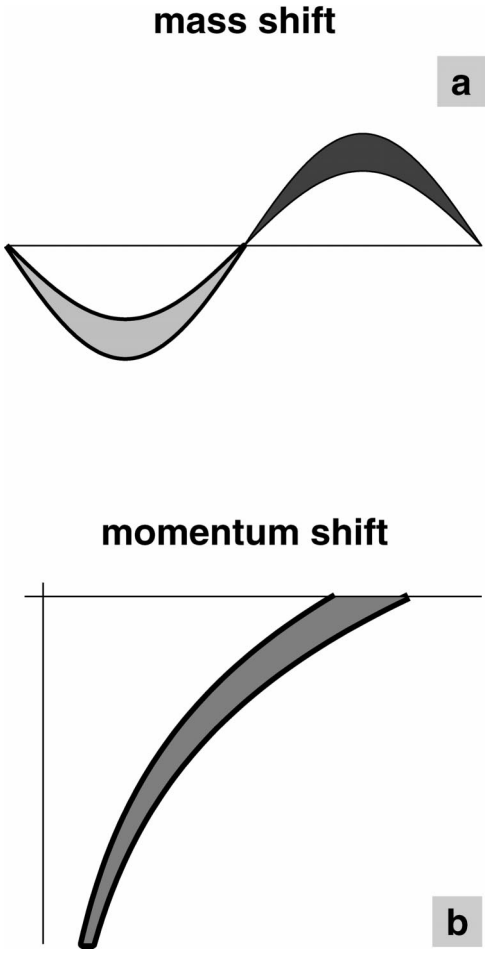

FIG. 1. Momentum conversion from periodic motion to mean motion during breaking. (a) Sketch of conversion due to shifted distribution of mass. (b) Sketch of mean momentum lost from the periodic motion $\hat{u}$ due to reduced velocities after breaking. The magnitudes of the amplitude reduction have been exaggerated in both panels. See the text for details.

of the wave motion in the water column must give rise to an interior adjustment of the mean current. Hence,

$$\rho\Delta\overline{u}_i = \frac{d}{dz}\overline{\Delta M_2}(z < \eta) = \rho c_0\varepsilon_0\Delta\varepsilon[(1 - \varepsilon_0^2)e^{2kz_0} + 2\varepsilon_0^2 e^{4kz_0}]. \quad (21)$$

To the lowest order in ε, the interior adjustment Δu_i is equal to one-half of the change of the Stokes drift which is induced by breaking.

6. Drift currents

For the mean current, the two-dimensional problem in which the horizontal current depends on the vertical coordinate and time will be considered. Moreover, in the present context, the drift of water particles (the Lagrangian drift) is different from the Eulerian velocities. The Eulerian problem given by (3) may be transformed to a Lagrangian problem using the relation

$$\overline{u}_L = \overline{u} + \overline{u}_S \quad (22)$$

(Phillips 1977). Then,

$$\frac{\partial\overline{u}_L}{\partial t} - \frac{\partial}{\partial z}\nu\frac{\partial\overline{u}_L}{\partial z} = \frac{\partial\overline{u}_S}{\partial t} - \frac{\partial}{\partial z}\nu\frac{\partial\overline{u}_S}{\partial z}, \quad (23)$$

where $\overline{u}_S$ is given by (15).

The wind stress in the atmospheric boundary layer is denoted by τ; that is,

$$\tau = \rho^{(a)}u_*^{(a)^2}, \quad (24)$$

where u_* is the friction velocity and the superscripts (a) denote atmospheric quantities. A significant amount of the momentum that is transferred from the atmosphere to the ocean contributes to wave growth (Melville and Rapp 1985; Weber and Melsom 1993a). The stress associated with such momentum transfer is here denoted by $\tau^{(w)}$, and f is introduced as the fraction of $\tau^{(w)}$ to the total wind stress τ; that is,

$$\tau^{(w)} = f\tau. \quad (25)$$

The boundary condition at the surface becomes

$$\frac{\partial\overline{u}_L}{\partial z}(z = 0) = \frac{\tau^{(o)}}{\rho\nu} + \frac{\partial\overline{u}_S}{\partial z}(z = 0), \quad (26)$$

where

$$\tau^{(o)}(t) = (1 - f)\tau + \tau_{\rm vw}(t - t_0). \quad (27)$$

Here, the virtual wave stress $\tau_{\rm vw}$ is given by (20), and t_0 is the time at which the latest wave breaking occurred. Note that, because of wave breaking, $\tau^{(o)}$ will be a function of time even in the case of a constant wind stress τ.

Momentum associated with the wave motion will be transformed to mean motion according to (21). Thus, the problem must be reinitialized:

$$\overline{u}_L^+ = \overline{u}_L^- + \Delta\overline{u}_i + \Delta\overline{u}_S, \quad (28)$$

where $\overline{u}_L^+$ and $\overline{u}_L^-$ are the drift profiles after the present wave breaking event and prior to the breaking event, respectively. The instantaneous adjustments $\Delta\overline{u}_i$ and $\Delta\overline{u}_S$ are given by (21) and (19), respectively. Given a boundary condition at the bottom or in the ocean's interior, the problem given by (23)–(28) may be solved.

Furthermore, note that, when T_b is the period between breaking events, we have

$$\int_{t_0}^{t_0+T_b}\tau_{\rm vw}\,dt' + \rho\int_{-\infty}^{0}\Delta\overline{u}_i\,dz' = T_b f\tau. \quad (29)$$

Thus, in the present formulation all of the momentum transfer from the atmosphere to the ocean is ultimately consumed by the ocean currents.

7. Results

One aim of the present paper is to provide realistic descriptions of effects of wave breaking on drift and turbulence. Nevertheless, in appendix B we include an analytical solution of the velocity perturbation due to a wave-breaking event, based on a constant-value eddy viscosity. There are two reasons for this: 1) to provide a preliminary assessment of steep waves on the drift induced by wave breaking and 2) to provide an exact solution that may be used to test a numerical description of the problem.

The full problem is given by (6) and (23) with surface boundary conditions (8) and (26). In the numerical formulation of the problem, conditions of the Neumann type are applied in the ocean's interior:

$$\frac{\partial}{\partial z}\overline{u}_L(z = -H) = 0 \quad \text{and} \quad \frac{\partial}{\partial z}q^2(z = -H) = 0, \quad (30)$$

where H is a depth that is large relative to the wave length. The initial condition for the drift is

$$\overline{u}_L(t = 0) = \overline{u}_S, \quad (31)$$

which correspond to a state of rest prior to the onset of wind forcing and waves at $t = 0$. Further, (re-)initialization of $\overline{u}_L$ after a wave-breaking event is given by (28). There is no obvious choice of initial condition for the turbulent kinetic energy. For simplicity, a constant-value initial background turbulence is assumed:

$$q^2(t = 0) = q_0^2, \quad (32)$$

which is generally in discord with the surface boundary condition (8). The initial background turbulence is set to a low value of $q_0^2 = 2 \times 10^{-6}$ m^2 s^{-2} (the results after 30 minutes turned out to be virtually independent of the initial value used for q_0^2).

Numerical integration is conveniently performed after invoking the transformation

$$y = \int_0^z \frac{dz'}{l(z')} \quad (33)$$

(see CB), which ensures that the surface boundary layer

is properly resolved. The equations are solved using a standard centrally differenced form with second-order accuracy in time and in the y domain. In (6) the shear production term is evaluated at the old time step. Moreover, the dissipation term is made up of two factors, q and q^2, where the former and latter factors are evaluated at the old time step and the new time step, respectively. In (23) values for q (and ν) in the diffusion term are computed from the old time step. Moreover, the temporal resolution is increased immediately after wave breaking in order to accurately describe the sudden impact of wave breaking on the mean motion. This approach is slightly different than the numerical method applied by CB. All profiles and time series that will be presented are computed as the temporal mean values between two events of wave breaking. Results quoted as obtained with a constant surface stress (in case 1 and case 2 below) are analogous to the results in CB.

In order to solve the problem, a number of parameter values must be specified. For the parameters related to turbulence closure, the values quoted in Table 1 in C96 are adopted; that is, $S_M = 0.39$, $S_q = 0.2$, $B = 16.6$, and $\kappa = 0.4$. Furthermore, we are faced with the ''rather unpleasant problem of estimating z_r'' (Madsen 1977). Here, the oceanic equivalent of the Charnock formula, that is,

$$z_r = \frac{au_*^2}{g}, \tag{34}$$

will be used. Based on an examination of the laboratory data presented by Cheung and Street (1988), C96 determines z_r by minimizing errors in the turbulence model. The results are presented in Table 2 in C96 and yield values for a in the range 250–2000. Based on interpretation of velocity profiles, Bye (1988) proposes that $a \approx O(10^3)$. Terray et al. (1996) find good agreement between their field observations and the turbulence model by CB if $z_r \sim H_S$; then, the results in Table 1 in Terray et al. yield $a \approx O(10^4)$ and $\alpha \approx O(10^2)$. Based on observational data from Knight Inlet, Stacey (1999) finds that $a \approx O(10^5)$ when $\alpha = 150$. The data that have been quoted here clearly indicate that a universal constant value of a does not exist, and one reason for this is that the surface roughness is a function of the sea state (Donelan 1990). Nevertheless, we believe that the use of (34) is justified in this rather idealized study. A case with a friction velocity $u_* = 0.018$ m s^{-1} will be examined here using $a = 2 \times 10^4$ and $\alpha = 100$. The oceanic surface roughness length then becomes $z_r = 0.66$ m.

In order to obtain a consistent specification of the sea state and the air–sea momentum transfer, a state-of-the-art wave model, WAM (Komen et al. 1994), was used. WAM models the temporal evolution of the directional wave spectrum, for waves with lower frequencies than a specified cutoff frequency. This frequency range is usually referred to as the dynamic range of wave frequencies. For higher frequencies than the cutoff value, WAM assumes a prescribed shape of the wave spectrum, which is usually referred to as the tail of the spectrum. The energy input from the wind to the tail of the spectrum is predominantly balanced by dissipation, giving rise to a continuous flux of turbulence at the surface.

We applied a constant wind forcing of 12 m s^{-1}, and inspected the results from WAM for the period 4–6 hours after the initialization. Then, the steepest waves had wave numbers in the range 0.13–0.2 m^{-1}, with the largest steepness being observed for longer waves as time progressed. The friction velocity u_* was in the range 0.18–0.19 m s^{-1}, with values that declined slowly with time. The steepness of the steepest waves was approximately 0.34, and f, the fraction of momentum transfer from the atmosphere that was generating waves in the dynamic range of the wave spectrum, declined from 0.56 to 0.47.

Based on these results from the WAM wave model, we set $u_* = 0.18$ m s^{-1}, $\varepsilon_0 = 0.34$, $\Delta\varepsilon = 0.0062$, $\zeta_0 = 2$ m, $T_b = 600$ s; g is set to 9.8 m s^{-2}. These values correspond to a wavelength of 37 m, and the nondimensional number in (A6) becomes $B_0 = 2 \times 10^{-4}$. Then, the reduction of wave energy due to a wave-breaking event is $2\Delta\varepsilon/\varepsilon_0 = 3.6\%$, which lies within the 1%–10% range indicated by the experimental results of Melville and Rapp (1985). Also, from (29) this specification implies that the fraction of the total atmospheric stress that contributes to wave growth is $f = 0.51$. This value complies with the results of Mitsuyasu (1985). If we specify the density of air by $\rho = 800\rho^{(a)}$, we have $u_*^{(a)} = 0.51$ m s^{-1}. The phase speed of the wave then becomes $c = \sqrt{g/k} = 7.6$ m s^{-1}, and the wave frequency is $\omega = kc = 1.3$ s^{-1}. Furthermore, the growth rate follows from the relation

$$\varepsilon_0 + \Delta\varepsilon = \varepsilon_0 e^{\beta T_b}. \tag{35}$$

We find that $\beta = 3.0 \times 10^{-5}$ s^{-1} and the steepness at wave breaking becomes $\varepsilon_0 \exp(\beta T_b) = 0.346$. Further, we define a nondimensional age of steep waves as $c/u_*^{(a)}$, where c is the phase speed of the waves whose momentum is partially transferred to the drift current when wave breaking occurs. Here, this nondimensional age is 14.9.

Because of the assumption of a constant atmospheric stress in a model without a momentum sink, and where effects of the earth's rotation are disregarded, we must impose a limit on the length of the time period for which our integrations will be performed. We have chosen to set this limit to 6 h, since effects of the earth's rotation will then be quite noticeable at most latitudes (see Fig. 4 in Melsom 1996).

Results from four cases will be examined. In this context, we will refer to results produced by setting $f = 0$ in (27) as the ''constant stress'' case since the surface stress $\tau^{(o)}$ in (27) then becomes time invariant. In this case, the wave amplitude is constant, and so the virtual wave stress vanishes, and there is no reinitiali-

zation according to (28). Results from the constant-stress case are derived identically to the CB theory when effects of the earth's rotation are disregarded. Thus, the profiles of Eulerian velocity and the scaling velocity for turbulence will be denoted as $\overline{u}_{\mathrm{CB}}$ and q_{CB}, respectively.

In the realistic case, with $f > 0$, $\tau^{(o)}$ becomes time dependent, and this will be referred to as the ''time-varying stress'' case. Results will be derived using both $O(\varepsilon^2)$ accuracy and $O(\varepsilon^4)$ accuracy in the present wave model, and the corresponding sets of profiles of Eulerian velocity, Lagrangian drift, and the scaling velocity for turbulence will be denoted as $\overline{u}_2$, $\overline{u}_{L;2}$, q_2 and $\overline{u}_4$, $\overline{u}_{L;4}$, q_4, respectively. As described above, $f = 0.51$ in the present specification of the sea state. Note that the TKE flux at the surface is parameterized by (8) throughout.

The cases that will be examined are defined below and will hereinafter be referred to by their case numbers:

- case 1: offsets in Eulerian velocities and TKE, when results due to a time-varying surface stress $\tau^{(o)}$ based on $O(\varepsilon^4)$ in the wave model ($\overline{u}_4$, q_4) are compared with results that are produced in the case of a constant stress ($\overline{u}_{\mathrm{CB}}$, q_{CB});
- case 2: as for case 1 but with $O(\varepsilon^2)$ accuracy in the wave model ($\overline{u}_4$, q_4 in case 1 is replaced by $\overline{u}_2$, q_2);
- case 3: offsets in Eulerian velocities when results based on the $O(\varepsilon^2)$ wave model ($\overline{u}_2$, q_2) are compared with the $O(\varepsilon^4)$ results ($\overline{u}_4$, q_4);
- case 4: as for case 3 but for the Lagrangian drift ($\overline{u}_2$, $\overline{u}_4$ in case 3 is replaced by $\overline{u}_{L;2}$, $\overline{u}_{L;4}$).

First, the temporal development of the results from case 1 and case 2 is examined. The results are depicted in Fig. 2. In Figs. 2a and 2b, these time series are shown for the depths of 0.4 and 4.9 m, respectively. Here, the black curves are the velocity time series, and the gray curves are the time series of the scaling velocity for turbulence (q), for a period of 6 h. Thick and thin lines correspond to offsets (in percent) from case 1 and case 2, respectively, and so the thick and the thin black lines in Fig. 2a display the temporal evolutions at $z = -0.4$ m of $100(\overline{u}_4 - \overline{u}_{\mathrm{CB}})/\overline{u}_{\mathrm{CB}}$ and $100(\overline{u}_2 - \overline{u}_{\mathrm{CB}})/\overline{u}_{\mathrm{CB}}$, respectively.

From Fig. 2, we note that the offset of q is nearly time independent for these near-surface levels in the present formulation. We also observe from Fig. 2a that the surface current derived using the $O(\varepsilon^4)$ wave model is larger than that for the $O(\varepsilon^2)$ model. This is due to the fact that the virtual wave stress is higher when the $O(\varepsilon^4)$ wave model is applied [see (20) and (17)]. The sum of surface stresses in (27) has a temporal dependence due to wave breaking, which necessarily leads to a higher level of mean kinetic energy than in the absence of wave breaking. For this reason it is expected that the surface current has a positive offset. Such an offset is displayed in Fig. 2a for case 1 and for case 2. The reduction of the wave breaking effects in time is due to the higher turbulent mixing near the surface in the presence of wave breaking.

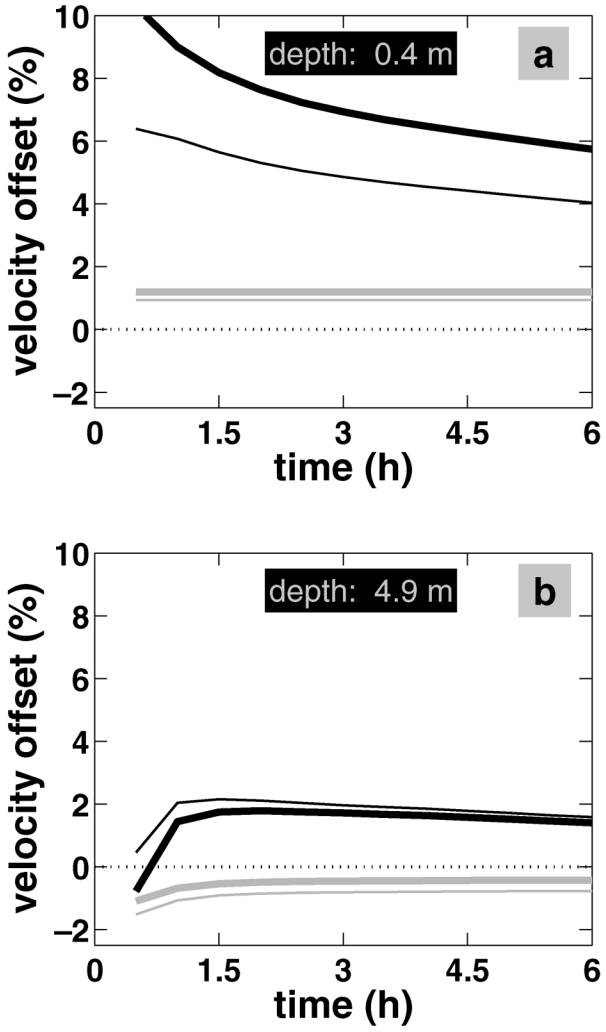

FIG. 2. Time series for offsets of $\overline{u}$ (black curves, mean current) and q (gray curves, scaling velocity for turbulence) due to a time-varying surface stress, as compared with the constant-surface-stress case. The offset in u is defined as $(\overline{u}_{4/2} - \overline{u}_{\mathrm{CB}})/\overline{u}_{\mathrm{CB}}$, and offsets in q are defined analogously. Numbers on the vertical and horizontal axes are offset values in percent and time in hours, respectively. [In (a), the gray lines overlap.] A box filter has been applied, with a length set to the period between two wave-breaking events (presently, this period is 5 min). Thick and thin lines correspond to computations based on $O(\varepsilon^4)$ and $O(\varepsilon^2)$ accuracy in the wave model, respectively. Here, ε is the wave steepness. (a) Time series for a node close to the surface (at $z = -0.4$ m) from the numerical solution. (b) Near-surface time series at $z = -4.9$ m. See the text for further details.

In Fig. 3a, profiles for offsets of mean current and the scaling velocity after 6 h of integration are depicted. The same convention for black and gray, thick and thin lines as in Fig. 2 was used. At first sight, Fig. 3a seems to indicate that the integrated momentum is larger when a time-varying surface stress is applied when compared with the constant-stress case. However, at all depths below approximately $z = -12$ m, the Eulerian mean

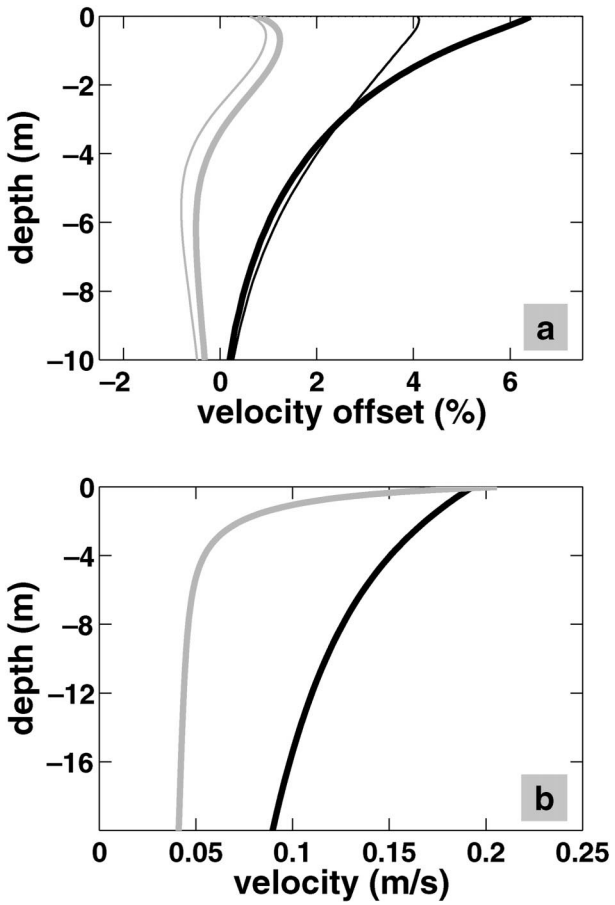

FIG. 3. (a) Profiles for offsets of $\overline{u}$ (black curves, mean current) and q (gray curves, scaling velocity for turbulence), as defined in the Fig. 2 caption. Numbers on the vertical and horizontal axes are vertical levels in meters and offsets in percent, respectively. Thick and thin lines display the same quantities as in Fig. 2. (b) Profiles of the Eulerian mean current ($\overline{u}_{\mathrm{CB}}$) and the scaling velocity for turbulence (q_{CB}), when $\tau^{(o)} = \rho u_*^2$ (and $f = 0$) in (27). In both (a) and (b), profiles are displayed after 6 h of integration.

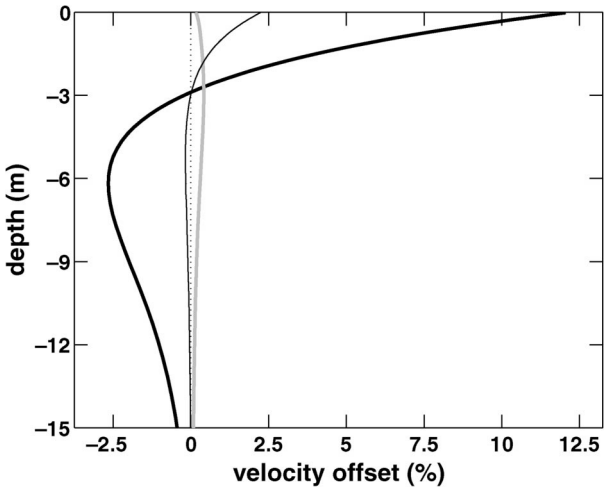

FIG. 4. Profiles for offsets of $\overline{u}$ (black curves, mean current) and q (gray curve, scaling velocity for turbulence). Here, results from wave theory with accuracy $O(\varepsilon^4)$ are compared with $O(\varepsilon^2)$ results, with a time-varying surface stress applied in both cases. Numbers on the vertical and horizontal axes are vertical levels in meters and offsets in percent, respectively. Thick and thin black lines correspond to differences in Lagrangian and Eulerian velocities, respectively. The Lagrangian velocity offset is defined as $(\overline{u}_{L;4} - \overline{u}_{L;2})/\overline{u}_{L;2}$, and the Eulerian offset becomes $(\overline{u}_4 - \overline{u}_2)/\overline{u}_2$. Profiles are displayed for the upper 15 m of the water column only, after 6 h of integration.

current offsets are negative, in compensation for the excess momentum near the surface. Obviously, the conservative property is the Lagrangian momentum. When the differences in initial conditions are taken into account for the various numerical integrations, the results remain consistent. After application of a constant stress $\tau^{(o)} = \rho u_*^2$ ($f = 0$, i.e., similar to the CB theory), the vertical profiles for the Eulerian mean current and the scaling velocity for turbulence after 6 h are displayed in Fig. 3b.

Next, we turn our attention to case 3 and case 4. The offsets are depicted in Fig. 4, for the same domain and at the same time as in Fig. 3a. The black curves are time series for offsets in the mean current, and the gray curve is the offset of the scaling velocity for turbulence (q). Thick and thin black lines correspond to offsets (in percent) for the Lagrangian drift (case 4) and the Eulerian current (case 3), respectively. The higher-order theory leads to an enhanced drift adjacent to the surface and a somewhat retarded drift immediately below. This is most noteworthy when the Lagrangian drift is considered in case 4, as expected from (15).

8. Discussion

First, we note that the results in this paper to a certain extent rely on the description of the wave motion. The description of the wave field was developed from irrotational theory, which follows from disregarding the stresses in (2). This is an approximation that to some degree limits the validity of the subsequent results. Nevertheless, this is the conventional approach when effects of waves on mean currents are studied (e.g., Leibovich and Radhakrishnan 1977). Moreover, this approach has been improved by expanding such theory to fourth-order accuracy in wave steepness. Obviously, for a brief interval around breaking the nonlinear terms cannot be neglected. This problem has been resolved here by including the bulk parameterization in section 5, which takes advantage of the principle of momentum conservation.

As noted by Drennan et al. (1992), the scaling wave number for TKE dissipation may be related to the peak of the slope spectrum, but this spectrum is very broad. We consider steep waves of relatively long wavelengths; hence a large part of the momentum flux from the wind is initially carried by shorter gravity waves. In the previous section, we defined a nondimensional age of the longer steep waves as $c/u_*^{(o)}$. In Fig. 5, offsets of the

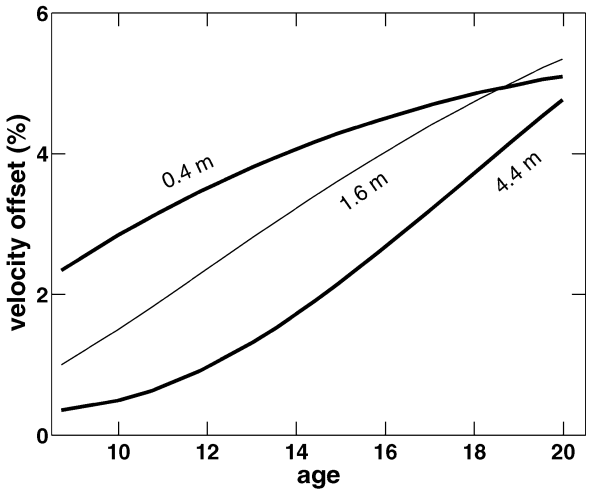

FIG. 5. Drift current offset $(\overline{u}_4 - \overline{u}_{CB})/\overline{u}_{CB}$ as a function of the nondimensional age of steep waves, after 6 h of integration. From top to bottom, the curves display the results at depths of 0.3 (thick line), 1 (thin line), and 3 m (thick line). With the exception of ζ_0 (and k), all parameter values have been retained from section 7.

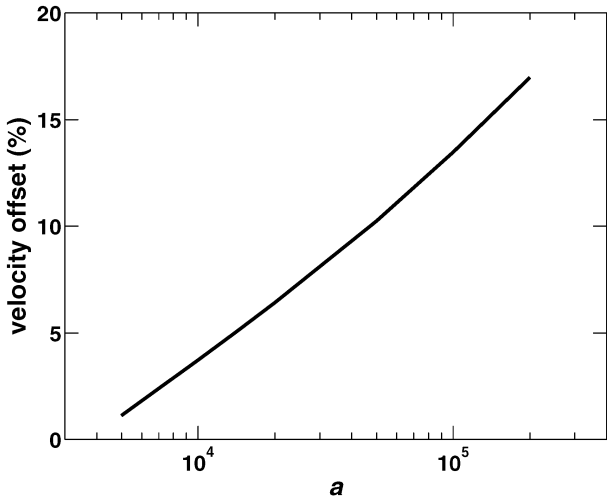

FIG. 6. Offsets $(\overline{u}_4 - \overline{u}_{CB})/\overline{u}_{CB}$ at the surface, as a function of the constant a in the Charnock formula, after 6 h of integration. The surface roughness z_r is proportional to a. With the exception of a (and z_r), all parameter values have been retained from section 7.

Eulerian mean currents at three selected depths are displayed as functions of the age parameter. Here, c should be interpreted as the phase speed of the steepest waves, whose momentum feeds the drift currents upon wave breaking. Hence, this is different from the conventional wave age parameter, which results from identifying c as the phase speed of the significant wave. For moderate wave ages, around 10, the significant wave has a steepness of about $\varepsilon_0 = 0.3$ (Sverdrup and Munk 1947). For larger wave ages, the steepness of the significant wave is smaller.

As seen from (8), a flux formulation has been applied as the surface boundary condition for the TKE. In the original closure theory, the surface TKE was set proportional to the surface stress (e.g., Mellor and Yamada 1982). The rationale for the flux formulation is that the TKE diffusion is directly influenced by this condition, and the TKE profile becomes more uniform near the surface. This occurs in response to mixing generated by surface gravity waves. Note that the implementation of a virtual wave stress in (20) does not replace the flux condition for the TKE in (8): Our study is limited to steep waves of relatively long wavelengths, whereas the dissipation of wave energy from the tail of the wave spectrum provides a source for the TKE flux at the surface.

In their study, Stacey and Pond (1997) found that the best results in a numerical simulation were obtained using the TKE flux condition (8). As noted by Stacey and Pond, the main weakness of the flux condition is that the roughness length enters as the surface value for the mixing length. We also note here that, in a recent study, Terray et al. (1999) found an improved model–data fit using an alternate length scale that is held constant at $-\kappa z_r$ above $-z_r$ and increases linearly below.

The surface roughness is a parameter that is frequently described with an unsatisfactory degree of perfection in ocean circulation problems. This study is no exception. In fact, we suspect that the surface roughness should be a function of time in the present formulation with highest values shortly after wave breaking has occurred. Nevertheless, since we are unaware of observational evidence of such behavior, any prescribed temporal development of z_r would be speculative. Other phenomena that are disregarded here, but that may well be important in the present context, include effects of swell (Donelan et al. 1997) and the three-dimensional response of breaking of waves with a finite crest length and nonsimultaneous wave-breaking events.

In order to assess the magnitude of differences due to the parameterization of the surface roughness, additional computations were performed using a wide range of values for the constant a in the Charnock formula (34). The increase in the velocity due to wave breaking was examined, and the results after 6 h of integration for the node closest to the surface are displayed in Fig. 6. For a given a, the increase in velocity due to wave breaking is generally rapidly reduced with depth, as shown in Fig. 3a.

In their study, CB find that, in the steady state, the shear production of turbulence is balanced by dissipation beneath a ''wave-enhanced surface layer.'' [In CB's terminology, the term ''wave-enhanced surface layer'' refers to the layer affected by the surface boundary condition (8).] When diffusion of turbulence is disregarded, and a time-varying stress $\tau^{(o)}$ is applied with $f = 0.51$ in (27), the surface velocity increases by about 20% when compared with the solution obtained with the full turbulence model. For the case of a constant stress $[\tau^{(o)} = \rho u_*^2]$, this value becomes approximately 24%. This difference is due to the relatively large velocity shears

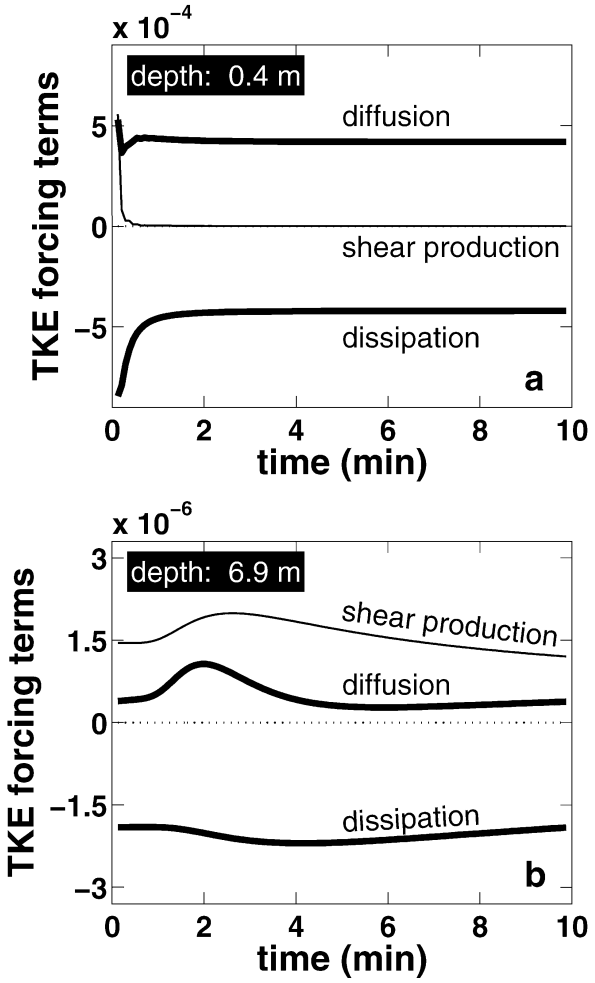

FIG. 7. Forcing terms for turbulent kinetic energy as a function of time after a wave-breaking event. From top to bottom, the curves in (a) show the development of the diffusion term (thick line), the shear production term (thin line), and the dissipation term (thick line), at a depth of 0.3 m. (b) The forcing terms at a depth of 5 m; the diffusion term is smaller than the production term. Numbers along the horizontal and vertical axes are time in minutes after a breaking event and magnitudes of terms in $m^2\ s^{-3}$, respectively (with the present choice of parameters, wave-breaking events occur with a period of 10 min).

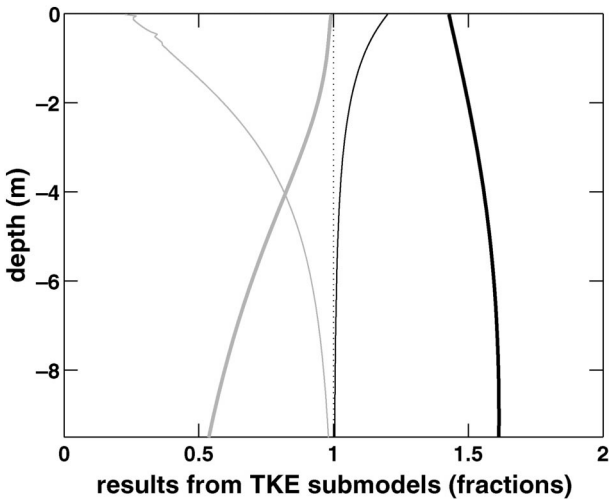

FIG. 8. Profiles for ratios of $\overline{u}_4$ (black curves, mean current) and q_4 (gray curve, scaling velocity for turbulence). Thick lines correspond to the ratio of the solution obtained with a dissipation–diffusion balance to the solution obtained with the full turbulence closure scheme. Thin lines show the corresponding ratios with the numerator replaced by the solution with the dissipation–shear production balance. Profiles after 6 h of integration are displayed for the upper 10 m.

that arise in the vertical direction when waves break. Hence, the presence of a ''wave-enhanced surface layer'' is confirmed, though slightly offset from the results that were reported by CB.

In order to further examine the details of near-surface turbulence in the context of a time-varying surface stress, the adjustment of the turbulence forcing terms in (6) was inspected. The evolution of the turbulence forcing terms is depicted in Fig. 7, as a function of time since a wave-breaking event occurred. From the results in Fig. 7a, we note that while the shear production term has a significant influence immediately after breaking at a depth of 0.4 m, there is a rapid adjustment to a diffusion–dissipation balance thereafter. These results help to explain the small differences between the present theory and the conventional approach and thus shed a new light on the success of the turbulence model by CB. Figure 7b shows that at a depth of 6.9 m, which is beneath the wave-enhanced surface layer, there is mainly a balance between the shear production term and the dissipation term, which is in agreement with CB.

In Fig. 8, results are displayed for the ratios of the solutions from two simplified turbulence models to results obtained with the full model. When omitting the shear production of turbulence (thick lines in Fig. 8), momentum mixing is reduced and the momentum becomes more trapped close to the surface. The current is increased by a factor of 1.35 at the surface. When the wind rotates in a nonaccelerating frame of reference as in CB (e.g., leading to the steady-state solution in their Fig. 7), the time-averaged vectorial momentum input from the wind during an inertial period vanishes. In the latter case, CB find that omitting shear production leads to a surface current that increases by a factor of about 1.4 (see the lower panel in their Fig. 6).

In the previous section, results were presented when the reduction of wave energy due to a wave-breaking event was set to 3.6%. After 6 h of integration, the Eulerian surface current was found to increase by 6.4% when a time-varying surface stress was imposed. When the reduction of wave energy is halved to 1.8%, the impact of the time-varying stress is even smaller, as the surface current enhancement becomes 3.4%.

Obviously, the impact of wave breaking on the near-surface velocity profile depends on the distribution of the air–sea momentum flux between waves and drift currents. In Fig. 9, the changes due to the presence of

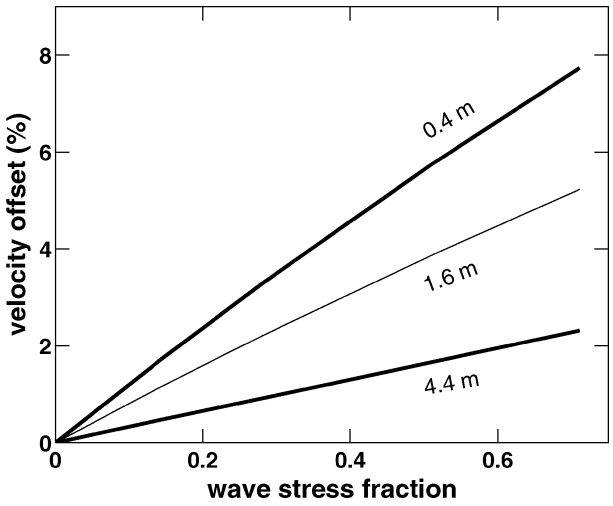

FIG. 9. Changes in the drift current offset $(\bar{u}_4 - \bar{u}_{CB})/\bar{u}_{CB}$ as a function of the fraction of the wind stress that induces wave growth [f in (25)]. From top to bottom, the curves display the results at depths of 0.3 (thick line), 1 (thin line), and 3 m (thick line). Various values of the fraction f were examined by changing the value of $\Delta\varepsilon$ (the change in wave steepness due to breaking). All other parameter values in section 7 were retained. Results are presented after 6 h of integration.

breaking waves are depicted as a function of the fraction of the wind stress that induces wave growth, that is, f in (25). We note that the changes are nearly a linear function of f and that the results converge toward the constant-stress case $f = 0$, that is, the theory of CB.

The work by CB and C96 on modeling the flux of TKE as proportional to the cube of the friction velocity has later been included in other studies of turbulence in the presence of breaking waves (e.g., D'Alessio et al. 1998). This approach has recently been extended to two-equation turbulence models by Burchard (2001). Our results indicate that the assumption of a constant stress $\tau^{(o)} = \rho u_*^2$ leads to only minor errors that are largest close to the surface. In the present paper, we have applied a physically sound bulk parameterization for isolated events of wave breaking. Thus, the errors that we report here constitute an assessment of the severity of applying the modified Mellor–Yamada model in a sea state where wave breaking is abundant. Since the errors we find are small, the present theory lends support to the use of the analytical solution from C96, as it was implemented by Burchard.

One purpose of the present investigation is to quantify errors in numerical ocean circulation models caused by ignoring the high-frequency variation of the surface stress $\tau^{(o)}$ that arises from wave breaking. From Fig. 3a, we observe that the errors in question extend only to a depth of a few meters. Even for this narrow range in depth, the error is small (a few percent). When the near-surface currents are of interest, the results may conceivably be improved by tuning the turbulence closure parameters. As noted by C96, the effect of diffusion on the TKE profile is mainly constrained to the region immediately beneath the surface. Alternative values for S_q were assessed by comparing the shapes and offsets of the profiles in case 1 statistically. However, the results were inconclusive, as, for example, a reduced value for S_q in the case $f = 0$ led to smaller offsets between the profiles, but a deterioration in the comparison of the shapes. Hence, we do not recommend modifications of S_q based on the present study. Note also that changing the value of S_q will affect the momentum sink at the bottom when a no-slip condition is applied at this boundary.

When the parameter values from section 7 are adopted, we find that the Lagrangian surface drift is enhanced by about 12% when effects of $O(\varepsilon^4)$ accuracy in wave steepness are included in the theoretical framework (case 4). This is the largest offset found in the present investigation, and also note the negative offsets at intermediate depths (see Fig. 4). For the chosen specification of the sea state, the Stokes drift increases by 14.45% when effects of $O(\varepsilon^4)$ accuracy are included (with an e-folding depth of 3.6 m), and this is why the Lagrangian surface drift is more affected than the Eulerian surface current. In relation to this, we note that in an investigation in which rotational effects are taken into account, Weber (1983) finds that the Stokes drift is reduced; see his Eq. (5.2). When the parameter values from section 7 are used in his theoretical result, we find that this reduction is approximately 6% at the surface (with an e-folding depth of about 0.18 m).

The effect of steep waves on the Stokes drift is worth notice. First, from (14) we observe that the Stokes transport is slightly enhanced as compared with traditional theory, by a factor of $\varepsilon^2/4$. Moreover, close to the surface the Stokes drift is also enhanced by steep waves. At the surface, the drift is increased by a factor of $1.25\varepsilon^2$. Using the theoretical limit for steepness of gravity waves, $\varepsilon \approx 0.44$ (e.g., Longuet-Higgins 1975), the limiting enhancement of the surface Stokes drift for steep waves is increased by a factor of about 0.24 when compared with the lowest-order result.

9. Conclusions

The present work is an investigation of the impact of repeated wave-breaking events on the near-surface profiles of velocity and TKE using an idealized, theoretical model. The model is idealized in the sense that it has been developed for monochromatic, irrotational surface waves with a uniform amplitude in a nonrotating, nonstratified fluid. The wave model is theoretical in a ''pure'' sense since waves are described using conservation laws throughout, and this principle is also adopted for the parameterization of effects of wave breaking through the bulk formulas in section 5.

The TCM that is employed is based on assumptions that are not satisfied when wave breaking is abundant. The turbulence theory has been developed for horizon-

tally homogeneous flows, and its calibration has been performed from data that are not representative for the present sea state. Still, CB find that adoption of the present TCM yields results that are in good agreement with observations. There can be little doubt that wave breaking is the circumstance in which the assumptions of the TCM are most severely violated. Hence, we provide results, when a physically sound parameterization of this circumstance is applied, in order to help bridge the gap from the turbulence theory and its intrinsic assumptions to its adaptation to a realistic sea state. When a realistic parameterization of effects of wave breaking is adopted, the near-surface profiles are only very modestly affected (by a few percent or less) when compared with the case in which the wave stress is disregarded. Hence, based on a theoretical wave model that uses a bulk formulation to parameterize wave-breaking events, we are able to shed light on the success of the turbulence model as it was reported by CB.

The small differences that we report were obtained when effects of wave breaking were magnified in a number of ways, and we will mention two issues that are of relevance in this context: First, all momentum lost in the process of wave breaking was assumed to be transferred to the mean motion. This reflects the idealized notion of a monochromatic wave field; in reality, a part of this momentum would be redistributed to waves with other frequencies. Second, we have expanded the traditional wave theory to fourth order in wave steepness, and this too is a source for larger differences from the conventional theory. Other higher-order effects, such as rotational theory, may give rise to adjustments that are opposite to the fourth-order theory corrections.

Acknowledgments. We thank Jan Erik Weber (Department of Geophysics, University of Oslo) and Jens Debernard (Norwegian Meteorological Institute) for valuable discussions and helpful advice. This work was made possible by the Research Council of Norway (Norges Forskningsråd) under Contract 121156/122. We are grateful for the financial support that has been provided by the council.

APPENDIX A

Inviscid Wave Motion

For two-dimensional plane waves traveling in the positive x direction in an infinitely deep inviscid fluid, the motion is governed by the Laplacian equation

$$\nabla^2\varphi = 0, \tag{A1}$$

where the velocity vector has been expressed as $\hat{\mathbf{v}} = \nabla\varphi$. A kinematic boundary condition is imposed at the top of the water column by assuming a material, free surface:

$$\frac{\partial\zeta}{\partial t} + \frac{\partial\varphi}{\partial x}\frac{\partial\zeta}{\partial x} = \frac{\partial\varphi}{\partial z}, \qquad z = \zeta. \tag{A2}$$

Furthermore, the motion must vanish at large depths, and so

$$\nabla\varphi \to 0, \qquad z \to -\infty, \tag{A3}$$

and the dynamical boundary condition at the free surface is

$$\frac{\partial\varphi}{\partial t} + \frac{1}{2}(\nabla\varphi)^2 + g\zeta = -P_s, \qquad z = \zeta, \tag{A4}$$

where $P_s = p_s/\rho$ and p_s is the pressure at the surface.

Solutions to the system (A1)–(A4) may be found by expanding the unknown variables in series after powers of the expansion parameter ε:

$$\psi = \sum_n \varepsilon^n \Psi_n. \tag{A5}$$

Here, ψ represents the unknown quantities φ, ζ, P_s, and $c = \omega/k$, and we choose $\varepsilon = k\zeta_0 e^{\beta t}$; that is, ε is the steepness of the gravest mode. In their discussion of observational data and analytic results, Weber and Melsom (1993b) find that $\beta/\omega \sim 10^{-4}$ or smaller. Hence,

$$\frac{\beta}{kc_0} = \varepsilon^2 B_0, \tag{A6}$$

where c_0 is the lowest-order approximation of the wave speed, and B_0 is a nondimensional number of order unity or less.

To the lowest four orders in ε, the periodic solution of this problem of exponentially growing waves with an initial gravest mode amplitude of ζ_0 becomes

$$\varphi = k^{-1}c_0\left[\varepsilon\sin\theta e^{kz} - \varepsilon^3\frac{1}{8}\sin\theta e^{kz} + \varepsilon^4\frac{1}{2}\sin(2\theta)e^{2kz}\right], \tag{A7}$$

$$\zeta = k^{-1}\left\{\varepsilon\cos\theta + \varepsilon^2\frac{1}{2}\cos(2\theta) + \varepsilon^3\left[\frac{3}{8}\cos(3\theta) + B_0\sin\theta\right] + \varepsilon^4\left[\frac{1}{3}\cos(4\theta) + \frac{17}{24}\cos(2\theta) + B_0\sin(2\theta)\right]\right\}, \tag{A8}$$

$$P_s = P_0 - \varepsilon^3 2c_0^2 B_0\sin\theta, \quad \text{and} \tag{A9}$$

$$c = c_0\left(1 + \varepsilon^2\frac{1}{2}\right). \tag{A10}$$

The dispersion relation may thus be written

$$\omega^2 = gk[1 + \varepsilon^2 + O(\varepsilon^4)] \tag{A11}$$

(e.g., Lamb 1932). Note that the solution given by (A7)–(A10) is positioned in the vertical direction by requiring that the surface at rest is situated at $z = 0$ [cf. Eq. (2) of Art. 250 in Lamb, where the mean surface is situated slightly above $z = 0$].

APPENDIX B

Analytical Solution

The effect of an event of wave breaking on the near-surface drift profile may be found by analytical means in the simple case of a constant eddy viscosity ν_0. The solution to lowest-order accuracy in wave steepness ε was calculated by Melsom (1996) for various specifications of the virtual wave stress τ_{vw}. Here, the virtual wave stress is assumed to act as an impulse, and so in (20),

$$F(t) = \delta(\omega t), \tag{B1}$$

where δ is the Dirac delta function. This problem is described by Melsom and constitutes a subproblem of the full formulation as given in section 6 in the present paper:

$$\frac{\partial u^{(\mathrm{br})}}{\partial t} - \nu_0 \frac{\partial^2 u^{(\mathrm{br})}}{\partial z^2} = 0,$$

$$\frac{\partial}{\partial z} u^{(\mathrm{br})}(z = 0) = \frac{\tau_{vw}(t)}{\rho \nu_0}, \quad \text{and}$$

$$u^{(\mathrm{br})}(t = 0) = \Delta u_i + \Delta u_S. \tag{B2}$$

The solution is obtained by Laplace transformation and subsequent inverse transformation, yielding

$$u^{(\mathrm{br})} = c_0 \Delta\varepsilon \left[\frac{1}{2}(\varepsilon_0 + \Delta\varepsilon + \varepsilon_0^3) \frac{e^{-z^2/(4\nu_0 t)}}{\sqrt{\pi k^2 \nu_0 t}} - \frac{4}{\pi} k(\varepsilon_0 + \Delta\varepsilon - 2\varepsilon_0^3) \int_0^\infty \frac{\cos(z\xi) e^{-\nu_0 t \xi^2}}{\xi^2 + 4k^2} \, d\xi - \frac{48}{\pi} k \varepsilon_0^3 \int_0^\infty \frac{\cos(z\xi) e^{-\nu_0 t \xi^2}}{\xi^2 + 16k^2} \, d\xi \right]. \tag{B3}$$

When only terms proportional to the lowest order in ε are kept, (B3) reduces to the solution in Melsom (1996) [see (21) in that paper]. Note that the expression above is not well defined for $t = 0$ because of the impulse imposed at the surface at this time. However, we have

$$\lim_{i \to 0} u^{(\mathrm{br})}(z < 0) = \Delta u_i + \Delta u_S \tag{B4}$$

in concord with the initial condition in (B2).

The temporal development and vertical profiles of $u^{(\mathrm{br})}$ are depicted in Melsom (1996) (to lowest order in ε; see Figs. 2a and 2b in that paper).

REFERENCES

Bleck, R., 2002: An oceanic general circulation model framed in hybrid isopycnic-Cartesian coordinates. *Ocean Modell.,* **4,** 55–88.

Burchard, H., 2001: Simulating the wave-enhanced layer under breaking surface waves with two-equation turbulence models. *J. Phys. Oceanogr.,* **31,** 3133–3145.

Bye, J. A. T., 1988: The coupling of wave drift and wind velocity profiles. *J. Mar. Res.,* **46,** 457–472.

Cheung, T. K., and R. L. Street, 1988: The turbulent layer in water at an air–water interface. *J. Fluid. Mech.,* **194,** 133–151.

Cox, M. D., and K. Bryan, 1984: A numerical model of the ventilated thermocline. *J. Phys. Oceanogr.,* **14,** 674–687.

Craig, P. D., 1996: Velocity profiles and surface roughness under breaking waves. *J. Geophys. Res.,* **101,** 1265–1277.

——, and M. L. Banner, 1994: Modeling wave-enhanced turbulence in the ocean surface layer. *J. Phys. Oceanogr.,* **24,** 2546–2559.

D'Alessio, S. J. D., K. Abdella, and N. A. McFarlane, 1998: A new second-order turbulence closure scheme for modeling the oceanic mixed layer. *J. Phys. Oceanogr.,* **28,** 1624–1641.

Donelan, M. A., 1990: Air–sea interaction. *The Sea: Ideas and Observations on Progress in the Study of the Seas,* B. LeMehaute and D. Hanes, Eds., Ocean Engineering Science, Vol. 9, John Wiley and Sons, 239–292.

——, W. M. Drennan, and K. B. Katsaros, 1997: The air–sea momentum flux in conditions of wind sea and swell. *J. Phys. Oceanogr.,* **27,** 2087–2099.

Drennan, W. M., K. K. Kahma, E. A. Terray, M. A. Donelan, and S. A. Kitaigorodskii, 1992: Observations of the enhancement of kinetic energy dissipation beneath breaking wind waves. *Breaking Waves,* M. L. Banner and R. H. J. Grimshaw, Eds., Springer Verlag, 95–101.

Hasselmann, K., 1970: Wave-driven inertial oscillations. *Geophys. Fluid Dyn.,* **1,** 463–502.

Komen, G., L. Cavaleri, M. Donelan, K. Hasselmann, S. Hasselmann, and P. A. E. M. Janssen, 1994: *Dynamics and Modelling of Ocean Waves.* Cambridge University Press, 532 pp.

Lamb, H., 1932: *Hydrodynamics.* 6th ed. Cambridge University Press, 738 pp.

Leibovich, S., and K. Radhakrishnan, 1977: On the evolution of the system of wind drift currents and Langmuir circulations in the ocean. Part 2: Structure of the Langmuir vortices. *J. Fluid Mech.,* **80,** 481–507.

Longuet-Higgins, M. S., 1969: A nonlinear mechanism for the generation of sea waves. *Proc. Roy. Soc. London,* **A311,** 371–389.

——, 1975: Integral properties of periodic gravity waves of finite amplitude. *Proc. Roy. Soc. London,* **A342,** 157–174.

Madsen, O. S., 1977: A realistic model of the wind-induced Ekman boundary layer. *J. Phys. Oceanogr.,* **7,** 248–255.

Mellor, G. L., 1973: Analytical prediction of the properties of stratified planetary surface layers. *J. Atmos. Sci.,* **30,** 1061–1069.

——, 1992: User's guide for a three-dimensional, primitive equation, numerical ocean model. Program of Atmospheric and Oceanic Sciences, Princeton University, 35 pp.

——, and T. Yamada, 1974: A hierarchy of turbulence closure models for planetary boundary layers. *J. Atmos. Sci.,* **31,** 1791–1806.

——, and ——, 1982: Development of a turbulence closure model for geophysical fluid problems. *Rev. Geophys. Space Phys.,* **20,** 851–875.

Melsom, A., 1996: Effects of wave breaking on the surface drift. *J. Geophys. Res.,* **101,** 12 071–12 078.

Melville, W. K., and R. J. Rapp, 1985: Momentum flux in breaking waves. *Nature,* **317,** 514–516.

Mitsuyasu, H., 1985: A note on the momentum transfer from wind to waves. *J. Geophys. Res.,* **90,** 3343–3345.

Phillips, O. M., 1977: *The Dynamics of the Upper Ocean.* 2d ed. Cambridge University Press, 336 pp.

Prandtl, L., 1952: *Essentials of Fluid Mechanics.* Hafner, 452 pp.

Song, Y., and D. Haidvogel, 1994: A semi-implicit ocean circulation model using a generalized topography-following coordinate system. *J. Comput. Phys.,* **115,** 228–244.

Stacey, W. M., 1999: Simulation of the wind-forced near-surface circulation in Knight Inlet: A parameterization of the roughness length. *J. Phys. Oceanogr.,* **29,** 1363–1367.

——, and S. Pond, 1997: On the Mellor–Yamada turbulence closure scheme: The surface boundary condition for q^2. *J. Phys. Oceanogr.,* **27,** 2081–2086.

Sverdrup, H. U., and W. H. Munk, 1947: Wind, sea and swell: Theory of relations for forecasting. Hydrographic Office Publication 601, U.S. Navy, 50 pp.

Terray, E. A., M. A. Donelan, Y. C. Agrawal, W. M. Drennan, K. K. Kahma, A. J. Williams III, P. A. Hwang, and S. A. Kitaigorodskii, 1996: Estimates of kinetic energy dissipation under breaking waves. *J. Phys. Oceanogr.*, **26,** 792–807.

——, W. M. Drennan, and M. A. Donelan, 1999: The vertical structure of shear and dissipation in the ocean surface layer. *The Wind-Driven Air–Sea Interface Electromagnetic and Acoustic Sensing, Wave Dynamics and Turbulent Fluxes*, M. L. Banner, Ed., ADFA Document Production Centre, 239–245.

Umlauf, L., and H. Burchard, 2003: A generic length-scale equation for geophysical turbulence models. *J. Mar. Res.*, **61,** 235–265.

Weber, J. E., 1983: Steady wind- and wave-induced currents in the open ocean. *J. Phys. Oceanogr.*, **13,** 524–530.

——, and A. Melsom, 1993a: Volume flux induced by wind and waves in a saturated sea. *J. Geophys. Res.*, **98,** 4739–4745.

——, and ——, 1993b: Transient ocean currents induced by wind and growing waves. *J. Phys. Oceanogr.*, **23,** 193–206.